



## City Research Online

### City, University of London Institutional Repository

---

**Citation:** Wang, J., Ma, Q. & Yan, S. (2018). A fully nonlinear numerical method for modeling wave-current interactions. *Journal of Computational Physics*, 369, pp. 173-190. doi: 10.1016/j.jcp.2018.04.057

This is the accepted version of the paper.

This version of the publication may differ from the final published version.

---

**Permanent repository link:** <https://openaccess.city.ac.uk/id/eprint/20340/>

**Link to published version:** <https://doi.org/10.1016/j.jcp.2018.04.057>

**Copyright:** City Research Online aims to make research outputs of City, University of London available to a wider audience. Copyright and Moral Rights remain with the author(s) and/or copyright holders. URLs from City Research Online may be freely distributed and linked to.

**Reuse:** Copies of full items can be used for personal research or study, educational, or not-for-profit purposes without prior permission or charge. Provided that the authors, title and full bibliographic details are credited, a hyperlink and/or URL is given for the original metadata page and the content is not changed in any way.

---

---

---

City Research Online:

<http://openaccess.city.ac.uk/>

[publications@city.ac.uk](mailto:publications@city.ac.uk)

---

# A Fully Nonlinear Numerical Method for Modelling Wave-Current Interactions

Jinghua Wang, Q.W. Ma\*, Shiqiang Yan

School of Mathematics, Computer Science and Engineering, City University of London, United Kingdom

## Abstract

The presence of current in the ocean can significantly modify the characteristics of ocean waves, and it is considered as an important factor responsible for the occurrence of extreme waves, e.g., rogue waves, which are well known as great threats to ocean engineering practices. The magnitude and direction of ocean current normally vary spatially and ocean waves can become very large and steep. Accurate and efficient phase-resolved numerical methods of fully nonlinear wave-current interactions on a large scale in three dimensions (3D) are required to understand their properties, but the existing phase-resolved methods are all based on the assumption of linear or weakly nonlinear interactions. This paper will address the issues and present a fully nonlinear numerical method to model the 3D interactions between waves and varying current on a large scale using a phase-resolved formulation. A new set of equations describing the three-dimensional, fully nonlinear interactions between waves and horizontally shearing current is proposed. They are derived by making no assumption on wave steepness or the order of wave-current interaction. The resulting new equations correctly describe the free surface boundary conditions by representing the fully nonlinear wave-current interactions, removing the limitation to the small wave steepness of the existing formulations in literature.

On this basis, the recently developed Enhanced Spectral Boundary Integral (short as ESBI) method is further enhanced to be able to model the wave-current interactions using the new equations, by developing the appropriate procedure for dealing with the extra terms related to nonlinear wave-current interactions. The new equations are used as the prognostic equations for updating the free surface in time domain, and a fast converging iterative technique is employed to solve them. The robustness of the newly developed method is demonstrated through comparing with experimental data available in literature and good agreements are observed in the several different cases, including the 3D fully interaction between ocean

\* Correspondence to: Northampton Square, Goswell Road, London, EC1V 0HN, UK

E-mail address: Q.Ma@city.ac.uk

waves and horizontally varying current. A comparison with a Higher Order Spectrum (HOS) method based on weak-nonlinear formulation of wave-current interaction is also made to confirm larger error does appear if the wave steepness is large. The method presented in the paper can be employed to simulate the real evolution of ocean waves on current in a phase-revolved way to give deep insights to the dynamics of wave-current interactions, which may not be done correctly by the existing methods so far.

*Keywords:* Wave-current interaction; Enhanced Spectral Boundary Integral method (ESBI); Random Seas; Rogue waves; Deep water; Large scale modelling; horizontally varying current, fully nonlinear simulation.

## 1 Introduction

When ocean waves encounter current, their properties, e.g., direction, speed, wave length and height, will be significantly modified. The current may affect the wave condition and increase the probabilities of the rogue wave occurrence [1], which are extreme waves of twice the significant wave height. Due to their abnormal dynamic features distinguished from the surrounding waves, rogue waves can impose great uncertainties on the safety of human's oceanic activities. Studies have pointed out that the ship accidents near the Agulhas current may be associated to the wave-current interactions [2, 3]. More recently, Lavrenov & Porubov [4] suggested that there are at least three reasons for rogue wave occurrence due to presence of current, i.e., a) wave energy amplification due to wave-current interaction, b) wave height amplification around a caustic due to refraction, and c) non-linear wave interaction in shallow water due to intersection of waves moving from different directions reflected by current. Therefore, accurate modelling of wave-current interactions is very important for the understanding of rogue wave mechanisms. In order to perform forecast and prevent impacts in advance in engineering practices, developing an efficient and accurate numerical tool to model wave-current interactions can be beneficial in practical perspective.

In many instances, the time and length scales of current are much larger than those of the waves, hence it is natural to assume the current is uniform in a local area [5]. To look at the local effects, many theoretical studies have investigated the interactions between a regular wave train with the uniform current [5-11], and good reviews can be found in [5] and [12]. Efforts have also been made to extend that to study the interaction between arbitrary (both regular and irregular) waves with the uniform current. Numerical wave tanks

(NWTs) are developed, e.g., those based on the shallow water equations [13-17], fully nonlinear Boundary Element Method [18-22] and Quasi-Arbitrary Lagrangian-Eulerian Finite Element Method [23], Fast Fourier Transform (short as FFT) based fully nonlinear Higher Order Spectrum (short as HOS) method [24] and Spectral Boundary Integral (short as SBI) model [25], and those based on the coupled continuity and Navier-Stokes equations [26-28].

Despite the success of those models for simulating the interactions between waves and the uniform current, the variation of the current in space cannot be considered by using them. The spatially varying current is often observed in real ocean environment and plays very important role in wave propagation on large scale, e.g., the large-scale variation of a current can change all the parameters describing a wave train as indicated by Peregrine [5]. To study the effects of varying current, the linear ray theory [29] is suggested, which can accurately predict the changes in wave length and direction due to refraction and blocking. However, it cannot predict the changes in the wave amplitude because waves become essentially nonlinear at the blocking point and therefore the linear solution is no longer accurate [22]. Although nonlinear theories describing the progressive waves riding on varying current are suggested [30-33] and fruitful results have been reported in recent studies [34-41], they can only be applied to regular waves or modulated uniform wave train [41], therefore such models are insufficient to describe random ocean waves consisting of components covering a wide range of spectra and subjected to spatially varying current. Nevertheless, an effective way to model random waves on varying current is through the phase-averaged models, which can provide useful statistical information, such as the spectra, etc. [42]. However, the specific wave kinematics and dynamics cannot be provided by the phase-averaged models due to the lack of the phase information, which are of great importance for precisely evaluating the responses and survivability of marine structures in real seas. Thus, the models in a phase-resolved approach are required.

Several phase-resolved models have been proposed. For example, the so-called Non-Linear Schrödinger Equation (short as NLSE) has been employed to study the current generated by a relatively small-amplitude slowly-varying internal long wave [43-48]. By using that, the effects of non-uniform current on the probability of rogue waves are explored, and it is found that the opposing current can cause rapid instability [46, 47]. Nevertheless, the NLSE is derived by assuming small wave steepness and narrow bandwidth, otherwise it becomes less accurate when applied beyond the limitations. The suitability of the NLSE for modelling random waves is discussed by Wang, et al. [49], in which the error of the NLSE has been quantified for simulating random waves. Due to such limitations, the NLSE will not be adopted in this study.

To avoid such drawbacks, the HOS method has been extended to consider the effects of slowly varying current in a weakly rotational media [50]. However, the formulations of this model are derived by expanding the parts representing the wave-current interactions in terms of the wave steepness, with neglecting the

higher order nonlinear terms. Although the method overcomes the limitation of narrow bandwidth imposed on the NLSEs, it is essentially weakly nonlinear for modelling wave-current interactions, and becomes less accurate when being used to simulate large steepness waves (more details will be given in the next section).

As restated, robust numerical modeling of wave-current interactions on large scale in two and three dimensions, while considering sufficient nonlinearities, can be useful to both applied science and engineering practices. However, the existing numerical models lack at least one of the following features: (i) modelling both regular and irregular waves in presence of current; (ii) simulating the current field that may be uniform or varying in space; (iii) being fully nonlinear and unassuming small wave steepness or narrow spectral bandwidth; (iv) being computationally efficient on large scale in both two and three dimensions. So far, the numerical method that can model the fully nonlinear interactions between waves and varying current on large scale in both two and three dimensions, possessing all the above features, has not been proposed to the best of the authors' knowledge. Therefore, to accurately model the effects of varying current on wave propagation on large scale becomes challenging due to the lack of such a powerful tool. This study successfully overcomes this challenge through three breakthroughs:

i) A new set of equations describing the 3D interactions between waves and varying current is developed, which is based on the fully nonlinear potential theory.

ii) The recently developed Enhanced Spectral Boundary Integral (short as ESBI) method [51-55], which has been demonstrated to be very efficient and accurate for simulating regular and irregular waves on both local and large scales [49, 56], is further extended for solving the new system of equations.

iii) A comprehensive validations are provided to show the robustness of the newly proposed theory and method through comparing with a variety of theoretical, numerical and experimental results available in literature.

In this way, the paper will describe a robust fully nonlinear numerical model to simulate interactions between waves and varying current. Accurate numerical simulations can be carried out by using this model in order to shed light on the impact of varying current on wave propagation on large scales, which can be beneficial to the community of applied scientists and ocean engineers and help them gain insights of the wave-current interactions for practical engineering applications.

## 2 Formulations and numerical implementations

To model the wave-current interactions numerically, some assumptions need to be made. Since significant contributions have been made in the earlier theoretical and numerical studies, the following assumptions adopted in those studies and shown to be effective are employed in this paper, e.g.,

i) One assumption in the aforementioned literature is that although the superposition of waves changes the current due to the mass flow induced by waves, the mass transport has negligible effects on the current field, especially in deep water. Hence, the feedback from waves to current can be ignored, and in such a way, the current field may be specified in advance [5]. Nevertheless, much progress has been made on studying the modification of the current fields by waves. It is reported that wave-induced Stokes drift affects the ocean boundary layer giving rise to widespread Langmuir circulation, which plays an important role in the air-sea interactions [57]. Very recently, Grue and Kolaas [58] pointed out that the waves induced Stokes drift is significantly higher than what is commonly represented in the wave-current interaction models, where the contribution of the boundary layer streaming should be incorporated.

ii) Another assumption is that the horizontal velocity of the current independent of the vertical coordinate [11, 43], which is based on the fact pointed out by Peregrine [5] that the characteristic time and length scale of the oceanic current is large compared with wind-waves.

iii) It is also assumed that such a flow is initially irrotational and will remain irrotational, hence velocity potential may be introduced and the potential theory can be employed [47].

Based on that, a set of formulations will be proposed below, which will be incorporated to the ESBI to model the fully nonlinear wave-current interactions.

## 2.1 Formulations describing wave-current interactions

All the variables used here have been non-dimensionalised, e.g., those in length are multiplied by peak wave number  $k_0$ , those in time by peak wave frequency  $\omega_0$ , velocity potential by  $k_0^2/\omega_0$  and velocity by  $k_0/\omega_0$ , where  $g$  is the gravitational acceleration, and the dispersion relation is given by  $\omega_0 = \sqrt{gk_0}$ .

The still water level is specified at  $Z = 0$ , while the free surface and velocity of the water can be split into two parts, i.e.,

$$\zeta = \bar{\eta} + \eta \quad (1)$$

$$\vec{u} = \vec{U} + (\nabla, \partial_z)\phi \quad (2)$$

where  $\nabla = (\partial_x, \partial_y)$  is the horizontal gradient operator,  $\vec{U} = (U, W)$  and  $\bar{\eta}$  are the current velocity and current induced surface elevation in absence of waves, respectively;  $\phi$  and  $\eta$  are the rest of the velocity potential and deflection of the free surface while involving the contribution of wave-current interactions.

As the current velocity  $\vec{U}$  is irrotational and time-independent, i.e.,  $\nabla \times \vec{U} = 0$  and  $\partial_T \vec{U} = 0$ . It is further assumed that the horizontal part of the current velocity is depth-independent in vicinity of the free surface, i.e.,  $\partial_Z U = 0$  within  $Z \in [-\delta L_0, \zeta]$ , where  $L_0$  is the peak wave length, and the velocity may or may not vary blow the level  $Z = -\delta L_0$ . If  $\delta \geq 1/2$ , it is understandable that the waves are not significantly affected

by the vertical variation of  $\mathbf{U}$ . Or in other words, the effects of the region below  $Z = -\delta L_0$  is insignificant to waves. Such assumption, i.e.,  $\partial_Z \mathbf{U} = 0$  within  $Z \in [-\delta L_0, \zeta]$  where  $\delta \geq 1/2$ , is reasonable approximation and often observed in real ocean [11, 43].

Hence, based on the potential theory, the governing equation and the corresponding boundary conditions can be given by,

$$\Delta \phi = 0, \text{ in } -\infty < Z \leq \zeta \quad (3)$$

$$\partial_T \zeta + \nabla \zeta \cdot (\mathbf{U} + \nabla \phi) - (W + \partial_Z \phi) = 0, \text{ at } Z = \zeta \quad (4)$$

$$\partial_T \phi + \zeta + \frac{1}{2} [(\mathbf{U} + \nabla \phi) \cdot (\mathbf{U} + \nabla \phi) + (W + \partial_Z \phi)^2] = 0, \text{ at } Z = \zeta \quad (5)$$

$$\partial_Z \phi = 0, \text{ at } Z \rightarrow -\infty \quad (6)$$

where  $\Delta$  is the Laplacian operator. It should be pointed out that the horizontal velocity of the current  $\mathbf{U}$  can be obtained from the measurement in-situ or in laboratory environment, however, it is difficult to acquire vertical velocity  $W$ . Nevertheless,  $W$  can be determined once  $\mathbf{U}$  is obtained, whereas one needs to utilize the boundary conditions in the current-only situation. When waves are absent, at  $Z = \bar{\eta}$ , the kinematic and dynamic boundary conditions can be derived as follows,

$$W(Z = \bar{\eta}) = \nabla \bar{\eta} \cdot \mathbf{U} \quad (7)$$

$$\bar{\eta} = -\frac{1}{2} (\mathbf{U} \cdot \mathbf{U} + W^2) \quad (8)$$

In addition, since  $\mathbf{U} = \mathbf{U}(\mathbf{X}) = \mathbf{U}(X, Y)$  and by using the irrotational condition  $\nabla \times \vec{U} = 0$ , one can obtain that

$$W = \nabla \cdot (\bar{\eta} \mathbf{U}) - Z \nabla \cdot \mathbf{U} \quad (9)$$

$$\bar{\eta} = -\frac{1}{2} [\mathbf{U} \cdot \mathbf{U} + (\nabla \bar{\eta} \cdot \mathbf{U})^2] \quad (10)$$

Unlike the cases subject to vertically shearing current, e.g., in reference [37], the nonzero vertical velocity  $W$  in this study is induced by horizontally varying current. Substitute Eqs. (9) and (10) into Eqs. (4) and (5), the surface boundary conditions can be reformulated as

$$\partial_T \eta + \nabla \zeta \cdot \nabla \tilde{\phi} - (1 + |\nabla \zeta|^2) \tilde{v} + \mu = 0 \quad (11)$$

$$\partial_T \tilde{\phi} + \eta + \frac{1}{2} [\nabla \tilde{\phi} \cdot \nabla \tilde{\phi} - (1 + |\nabla \zeta|^2) \tilde{v}^2] + \psi = 0 \quad (12)$$

where the tilde indicates the value at free surface, i.e.,  $\tilde{\phi} = \phi|_{z=\zeta}$ ,  $\tilde{v} = \partial_z \phi|_{z=\zeta}$ , and the terms representing the current effects are given by

$$\begin{pmatrix} \mu \\ \psi \end{pmatrix} = U_1 + U_2 \quad (13)$$

where

$$U_1 = \begin{pmatrix} \nabla \eta \cdot \mathbf{U} \\ \nabla \tilde{\phi} \cdot \mathbf{U} \end{pmatrix} \quad (14)$$

$$U_2 = \begin{pmatrix} \eta(\nabla \cdot \mathbf{U}) \\ -\eta(\nabla \tilde{\eta} \cdot \mathbf{U})\nabla \cdot \mathbf{U} + \frac{1}{2}(\eta \nabla \cdot \mathbf{U})^2 \end{pmatrix} \quad (15)$$

It is emphasized that Eqs. (14) represents the effects of the uniformity of the current, whereas Eqs.(15) denotes the influences of the variation of the current field. If the current field is uniformly distributed, then  $U_2 = 0$  and the system becomes the one used in the HOS [24] and the original SBI model [25]. Furthermore, it is pointed out that Eqs.(11) ~ (13) differ from that derived by Wu [50]. In Wu's formulations, they assumed that the horizontal velocity of the current slowly varies along the vertical direction, i.e.,  $\partial_z \mathbf{U} \sim O(\varepsilon)$ , where  $\varepsilon$  is the wave steepness, with  $\mathbf{U}$  and  $W$  expanded in terms of wave steepness and with the higher order terms of wave steepness, i.e.,  $\geq O(\varepsilon^2)$ , neglected when deriving  $(\mu, \psi)$ . Therefore, their approximation to the wave-current interactions is not fully nonlinear but only accurate to the first order of wave steepness, i.e.,  $\sim O(\varepsilon)$ , even for the uniform current. Their neglecting terms may not be significant for small and moderate waves but will become pronounced when the steepness of the simulated waves is large. The new approach of this paper based on Eqs. (11) ~ (15) overcomes this drawback and is fully nonlinear without such limitation on the wave steepness, hence are more accurate for describing the effects of varying current on wave propagation.

## 2.2 Implementation in ESBI

### 2.2.1 The prognostic equation

Now introducing  $V = \partial_n \phi \sqrt{1 + |\nabla \zeta|^2}$ ,  $\vec{n}$  is the outwards unit vector normal to the surface, Eqs.(11) and (12) can be rewritten as

$$\partial_T \eta = V - \mu = V - \nabla \eta \cdot \mathbf{U} - \eta(\nabla \cdot \mathbf{U}) \quad (16)$$

$$\partial_T \tilde{\phi} + \eta + \frac{1}{2} \left( |\nabla \tilde{\phi}|^2 - \frac{(V + \nabla \zeta \cdot \nabla \tilde{\phi})^2}{1 + |\nabla \zeta|^2} \right) + \psi = 0 \quad (17)$$

Eqs. (16) and (17) will be used as the prognostic equation for the ESBI method. Compared with the formulation in [55], there are two extra terms  $\mu$  and  $\psi$  in Eq. (16) and the  $\zeta$ -term in Eq. (17) is the total

free surface elevation including the part induced by the steady current. Apply Fourier transform to Eqs.(16) and (17), it can be obtained as

$$\partial_T \vec{M} + A \vec{M} = \vec{N} \quad (18)$$

where

$$\vec{M} = \begin{pmatrix} KF\{\eta\} \\ K\Omega F\{\tilde{\phi}\} \end{pmatrix}, A = \begin{bmatrix} 0 & -\Omega \\ \Omega & 0 \end{bmatrix} \text{ and } \vec{N} = \begin{pmatrix} KF\{G'_1\} \\ K\Omega F\{G'_2\} \end{pmatrix} \quad (19)$$

$F\{*\} = \int * e^{-i\mathbf{K}\cdot\mathbf{X}} d\mathbf{X}$  is the Fourier transform and  $F^{-1}\{*\}$  denotes the inverse transform,  $\mathbf{K}$  is the wave number in Fourier space and  $K = |\mathbf{K}|$ , the frequency  $\Omega = \sqrt{K}$ , and

$$F\{G'_1\} = F\{V\} - KF\{\tilde{\phi}\} - F\{\mu\} \quad (20)$$

$$F\{G'_2\} = \frac{1}{2} F \left\{ \frac{(V + \nabla\zeta \cdot \nabla\tilde{\phi})^2}{1 + |\nabla\zeta|^2} - |\nabla\tilde{\phi}|^2 \right\} - F\{\psi\} \quad (21)$$

The solution to Eq.(18) can be given as

$$\vec{M}(T) = e^{-A(T-T_0)} \left[ \int_{T_0}^T e^{A(T-T_0)} \vec{N} dT + \vec{M}(T_0) \right] \quad (22)$$

where

$$e^{A\Delta T} = \begin{bmatrix} \cos \Omega\Delta T & -\sin \Omega\Delta T \\ \sin \Omega\Delta T & \cos \Omega\Delta T \end{bmatrix} \quad (23)$$

The integration of Eqs.(22 ~ 23) is so robust that any Runge-Kutta method will work well. In this study, they are solved by using the fifth order Runge-Kutta method with adaptive time step, which has been shown very effective for modelling both regular and irregular waves [52, 55]. In addition, the wave generation and absorption are achieved by introducing an additional source term in Eq. (22), of which the details are omitted here for brevity but can be found in [53, 59].

### 2.2.2 Solution to the boundary integral equation

Meanwhile, one needs to solve the Laplace equation in order to determine  $V$ , which can be transferred to a boundary integral equation using the Green's theorem, i.e.,

$$\iint_S \frac{1}{r} \partial_n \phi' dS' = 2\pi\tilde{\phi} + \iint_S \tilde{\phi}' \partial_n \left( \frac{1}{r} \right) dS' \quad (24)$$

where  $S$  is the segment of the instantaneous free surface, the variables with the prime indicate those at source point  $(\mathbf{X}', Z')$ , the variables without the prime are those at field point  $(\mathbf{X}, Z)$ ,  $r = \sqrt{R^2 + (Z' - Z)^2}$  and  $R = |\mathbf{R}| = |\mathbf{X}' - \mathbf{X}|$ . Introducing  $dS' = \sqrt{1 + |\nabla\zeta|^2} d\mathbf{X}'$ , the above integral can be written as

$$\int_{S_0} \frac{V'}{r} d\mathbf{X}' = 2\pi\tilde{\phi} + \int_{S_0} \tilde{\phi}' \sqrt{1 + |\nabla'\zeta'|^2} \partial_n \left( \frac{1}{r} \right) d\mathbf{X}' \quad (25)$$

where  $S_0$  is the projection of  $S$  on to the horizontal plane, after introducing a new variable  $D = (\zeta' - \zeta)/R$ , the above equation becomes

$$\begin{aligned} \int_{S_0} \frac{V'}{R} d\mathbf{X}' &= 2\pi\tilde{\phi} + \int_{S_0} (\zeta' - \zeta) \nabla' \tilde{\phi}' \cdot \nabla' \frac{1}{R} d\mathbf{X}' \\ &\quad - \int_{S_0} \tilde{\phi}' \left[ \frac{1}{(1 + D^2)^{3/2}} - 1 \right] \nabla' \cdot \left[ (\zeta' - \zeta) \nabla' \frac{1}{R} \right] d\mathbf{X}' \\ &\quad - \int_{S_0} \frac{V'}{R} \left( \frac{1}{\sqrt{1 + D^2}} - 1 \right) d\mathbf{X}' \end{aligned} \quad (26)$$

The evaluation of  $V$  can be achieved by using the boundary integral equation, and it can be split into four parts in terms of different degrees of nonlinearities, i.e.,  $V = V_1 + V_2 + V_3 + V_4$ , where

$$V_1 = F^{-1} \{ KF \{ \tilde{\phi} \} \} \quad (27)$$

$$V_2 = -F^{-1} \{ KF \{ \zeta V_1 \} \} - \nabla \cdot (\zeta \nabla \tilde{\phi}) \quad (28)$$

$$V_3 = F^{-1} \left\{ \frac{K}{2\pi} F \left\{ \int \tilde{\phi}' \left[ 1 - \frac{1}{(1 + D^2)^{3/2}} \right] \nabla' \cdot \left[ (\zeta' - \zeta) \nabla' \frac{1}{R} \right] d\mathbf{X}' \right\} \right\} \quad (29)$$

$$V_4 = F^{-1} \left\{ \frac{K}{2\pi} F \left\{ \int \frac{V'}{R} \left( 1 - \frac{1}{\sqrt{1 + D^2}} \right) d\mathbf{X}' \right\} \right\} \quad (30)$$

It should be noted that Eqs.(24 ~ 30) slightly differ from those derived by Clamond and Grue [51], as  $\zeta$  here includes all the surface elevations due to current, waves and their interaction, rather than those due only to waves. Note that the dominant part of  $V_4$  can be further written into third order convolutions, of which the calculation is fast owing to the Fast Fourier Transform (FFT). Otherwise, the estimation of the remaining integration part of  $V_3$  and  $V_4$  are relatively slow. Later, Wang & Ma [55] suggested three techniques to improve the efficiency of the model, where a de-singularity method, a de-aliasing approach and convolutions up to 7<sup>th</sup> order for evaluating  $V$  are introduced, i.e.,

$$V_3 = \underbrace{V_3^{(1)}}_{4th \ convolution} + \underbrace{V_3^{(2)}}_{6th \ convolution} + \underbrace{V_{3,I}}_{integration} \quad (31)$$

$$V_4 = \underbrace{V_4^{(1)}}_{3rd \ convolution} + \underbrace{V_4^{(2)}}_{5th \ convolution} + \underbrace{V_4^{(3)}}_{7th \ convolution} + \underbrace{V_{4,I}}_{integration} \quad (32)$$

where the formulations for  $V_3$  and  $V_4$  can be found in the appendix. The integration terms are insignificant thus can be neglected when the wave steepness is small, but will be included in the calculation automatically

when wave steepness becomes sufficiently large. Through such a scheme, the high performance of the ESBI model can be guaranteed for simulating wave-current interactions both accurately and efficiently.

Note that the formulations in this section differ from that used by the original SBI [25], which is proposed to model the interaction between waves and uniform current. If not considering the variation of the current,  $\bar{\eta}$  becomes a constant reference level and can be taken as zero, thus  $\zeta = \eta$ ,  $\tilde{\phi} = \phi|_{z=\eta}$ , and the Eq.(27), (28) and (A.4) are identical to that in [25]. However, the original SBI [25] only considers the nonlinearities up to the third order for evaluating the vertical velocity, i.e.,  $V = V_1 + V_2 + V_4^{(1)}$ , of which the limitations have been discussed in [49]. Though for the applications in Grue and Jensen [25], the full and the cubic contribution gave the same result of the orbital velocity, the same conclusion may not be true in a time integration of the wave-current interactions. Nevertheless, the present model doesn't have such limitations for modelling the interactions between waves and uniform current.

### 2.2.3 Numerical technique for estimating $\bar{\eta}$

It should be emphasized that the current induced free surface  $\bar{\eta}$  in Eq. (10) is implicit and its estimation is not straightforward. However, it can be derived numerically. It is assumed that  $\bar{\eta} = \bar{\eta}_0 + \bar{\eta}'$ , where

$$\bar{\eta}_0 = -\frac{1}{2}\mathbf{U} \cdot \mathbf{U} \quad (33)$$

$$\bar{\eta}'(\bar{\eta}) = -\frac{1}{2}(\nabla\bar{\eta} \cdot \mathbf{U})^2 \quad (34)$$

In the equations,  $\bar{\eta}_0$  is determined by the velocity whereas  $\bar{\eta}'$  is a function of  $\bar{\eta}$ , and thus to determine  $\bar{\eta}$  in terms of  $\mathbf{U}$ , iterations are required through the following steps:

- 1)  $\bar{\eta}_{iter=0} = \bar{\eta}_0$ ;
- 2)  $\bar{\eta}_{iter+1} = \bar{\eta}_0 + \bar{\eta}'(\bar{\eta}_{iter})$ ,  $iter = iter + 1$ ;
- 3) Estimate the error between  $\bar{\eta}_{iter+1}$  and  $\bar{\eta}_{iter}$ , and examine the error: if error is less than the tolerance, the iteration can be terminated, otherwise go back to step 2).

Based on the techniques introduced in section 2.2.1-2.2.3, a flow chart illustrating the numerical implementation of the present model is shown in Figure 1.

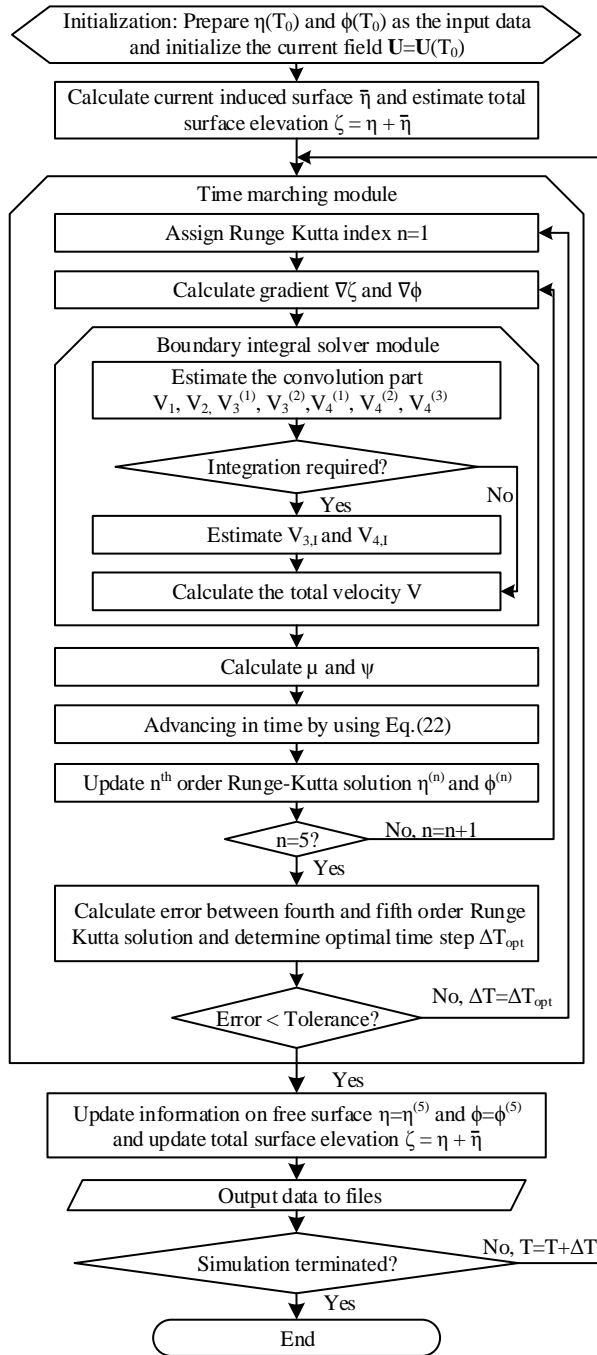


Figure 1. Flow chart of the implementation of present model

### 3 Validations

In order to demonstrate the effectiveness of the improved ESBI method for modelling the wave-current interactions, some numerical simulations are performed in this section and the obtained results are compared with the data in relevant literature.

#### 3.1 Uniform current

Since a regular wave train on uniform current behaves similarly to that on spatially-varying current, the case for it will be demonstrated in the section 3.2. Here firstly, a focusing wave on the uniform current is simulated. The results are compared with the laboratory measurements in Wu & Yao [60], in which the focusing wave is generated by using the formula

$$\eta_R = \sum_{n=1}^N a_n \cos(k_n X - \omega_n T + \theta_n) \quad (35)$$

where  $a_n$ ,  $k_n$  and  $\omega_n$  are the amplitude, wave number and frequency of each individual component,  $\theta_n = -k_n X_f + \omega_n T_f$ ,  $X_f$  and  $T_f$  are specified focusing location and time respectively.

The computational domain covers 32 peak wave lengths, and is resolved into 1024 points. A pneumatic wave maker is placed in the centre of the tank and the generated waves propagate towards both ends where they are absorbed. The information of the components, such as  $a_n$ ,  $k_n$  and  $\omega_n$ , etc., are extracted from the time history of the free surface in absence of the current in the literature. They are adjusted through iterations to minimize the error of the present model for reproducing the same focusing wave measured in laboratory. Next, with the calibrated components, two cases with following and opposing current are performed, where the velocity is  $\pm 0.1$ m/s. The time histories obtained by using the ESBI recorded at the focusing location, in comparison with the one observed in laboratory, are displayed in Figure 2. It shows that due to the wave-current interactions, the release of the wave packet on the following current was lagged, while this feature was reversed on the opposing current. Nevertheless, the results obtained by using the ESBI agree quite well with that recorded in the laboratory by Wu & Yao [60], where the errors of the maximum crest are 7% and 10% for following and opposing current, respectively, which indicates that the ESBI can be used to accurately model the wave interacting with the uniform current.

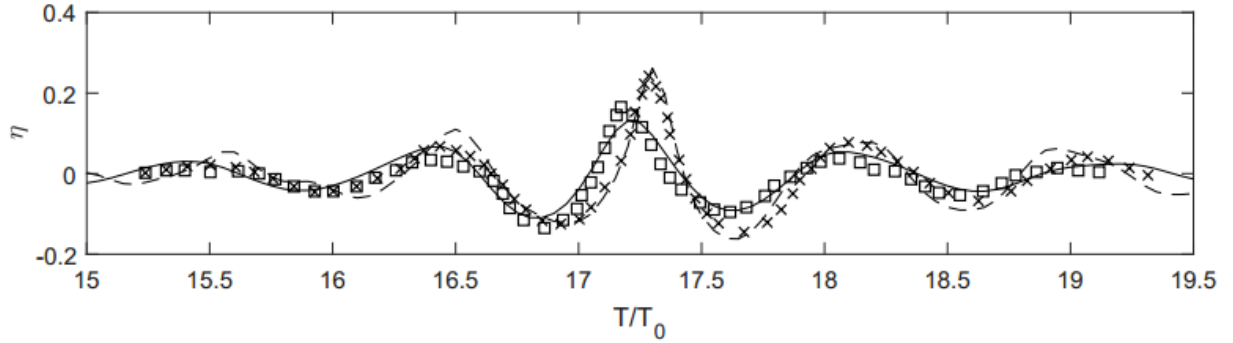


Figure 2. Comparison of the time history of free surface: rogue wave on uniform current. '- -': ESBI,  $U = 0.1\text{m/s}$ ; 'x': Wu and Yao [60],  $U = 0.1\text{m/s}$ ; '-': ESBI,  $U = -0.1\text{m/s}$ ; '—': Wu and Yao [60],  $U = -0.1\text{m/s}$

### 3.2 Two-dimensional spatially-varying current

In this subsection, the newly developed ESBI is employed to simulate two-dimensional uniform waves propagating on spatially-varying current. The obtained results are then compared with those by using HOS and those observed in laboratory to further validate the method.

#### 3.2.1 Regular waves on collinear current

The numerical simulations by using HOS in Wu [50] are performed here by using the newly developed ESBI model. The domain covers 256 wave lengths and 8192 points are used. The current profile is given by

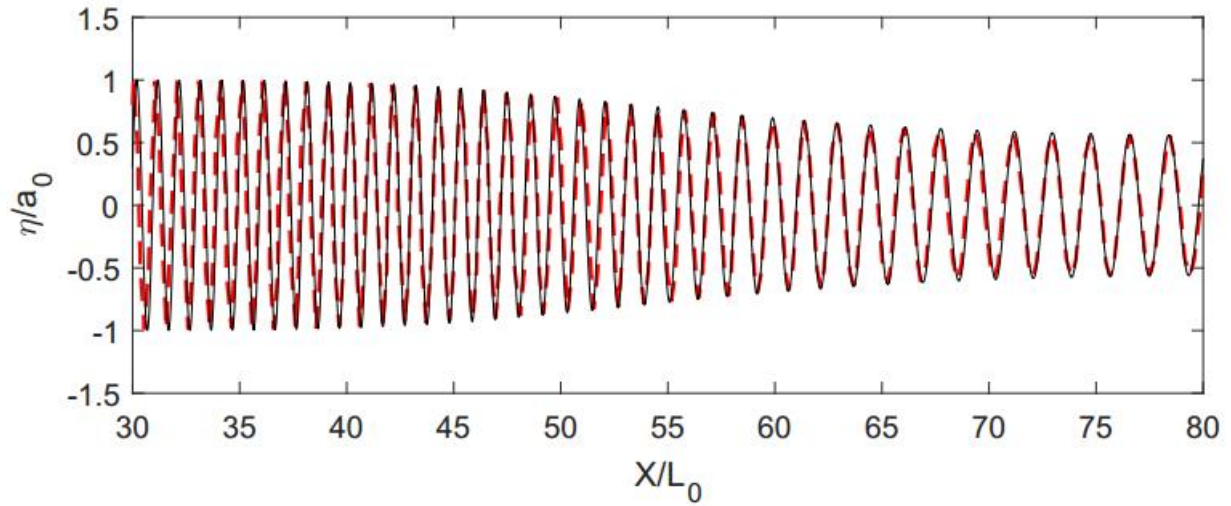
$$\mathbf{U}(X, Y) = \begin{cases} 0, & 0 \leq X \leq 24L_0 \\ U_m H((96L_0 - X)/72L_0), & 24L_0 < X \leq 96L_0 \\ U_m, & 96L_0 < X \leq 160L_0 \\ U_m H((X - 160L_0)/72L_0), & 160L_0 < X \leq 232L_0 \\ 0, & 232L_0 < X \leq 256L_0 \end{cases} \quad (36)$$

and  $H(\cdot)$  is the Hermitian polynomial,

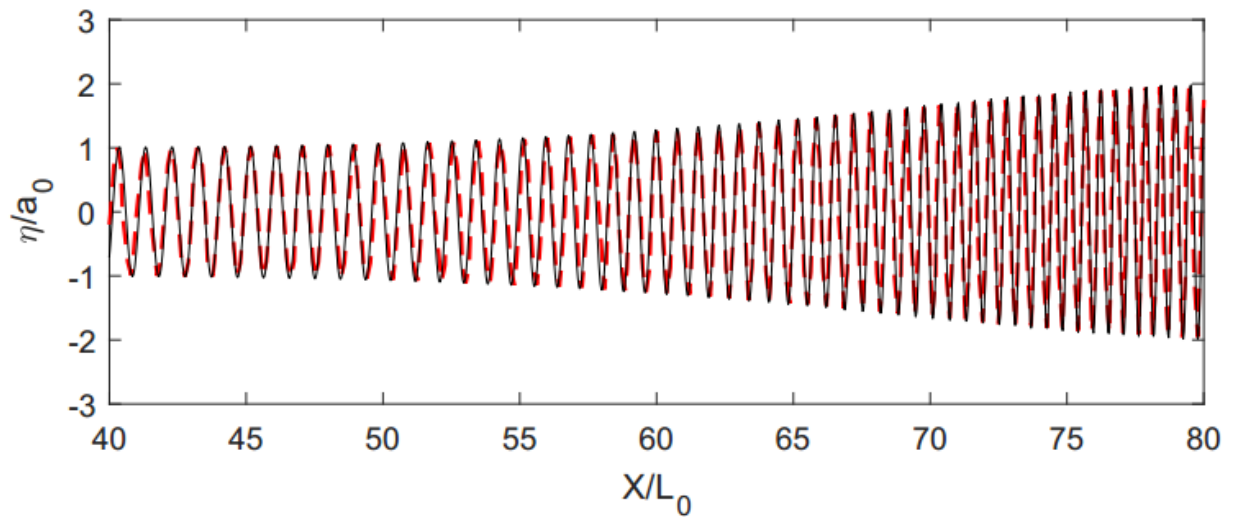
$$H(\xi) = 1 - 462\xi^6 + 1980\xi^7 - 3465\xi^8 + 3080\xi^9 - 1386\xi^{10} + 252\xi^{11} \quad (37)$$

Both cases of following and opposing currents are considered, i.e.,  $U_m/c_0 = 0.5$  and  $U_m/c_0 = -0.2$ , where  $c_0$  is the wave phase speed. The computational domain is initialized by a spatially-periodical Stokes wave train with steepness of 0.001 for linear waves and 0.2 for nonlinear waves, with simultaneous presence of current. Due to the current effects, the local wave steepness will be changed gradually with time, and it is found that the waves are not stabilized until 250 periods. Meanwhile, for the case of wave steepness 0.2

subjected to opposing current, wave breaking is observed due to the amplification effects induced by the opposing current. Thus, the initial steepness is adjusted to 0.05 to avoid the wave breaking. The stabilized free surface at the end of the simulation, in comparison with the surface elevation extracted from [50] is shown in Figure 3, where good agreement is observed.



(a) following current,  $U_m/c_0 = 0.5$



(b) opposing current,  $U_m/c_0 = -0.2$

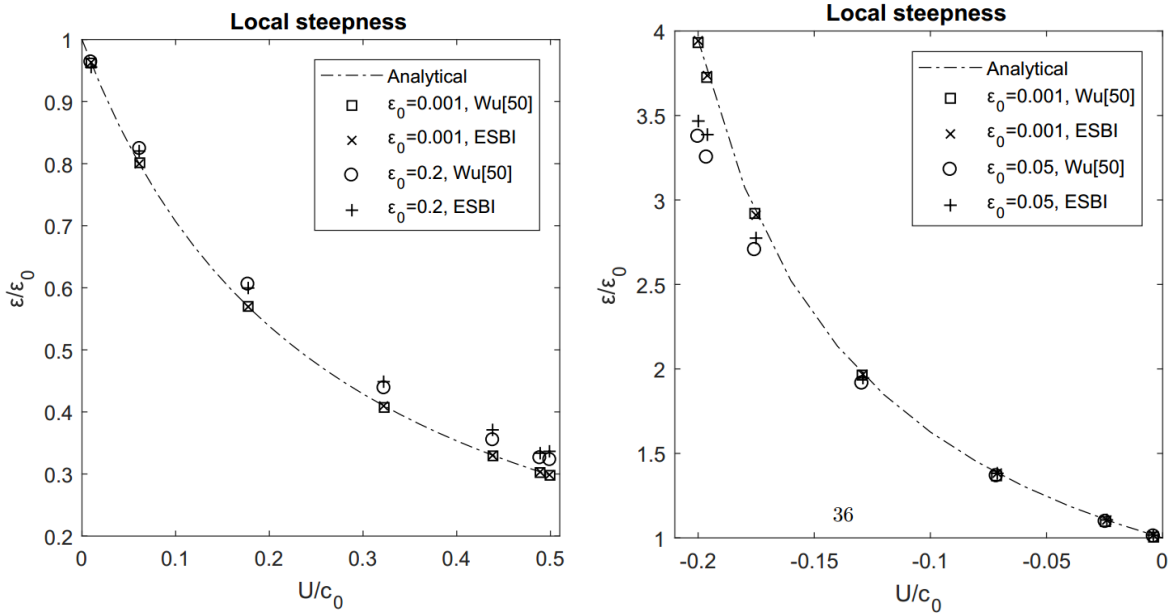
Figure 3. Comparison of the free surface in space: regular waves of steepness 0.001 on collinear current. '- - -': Numerical results in [50]; '-': Results by ESBI

To further demonstrate the effectiveness of the ESBI for this case, the local wave amplitude and wave number are estimated by using [60]

$$a_l = \sqrt{\eta^2 + \eta_H^2} \quad \text{and} \quad k_l = \frac{\eta \partial_T \eta_H - \eta_H \partial_T \eta}{\eta^2 + \eta_H^2} \quad (38)$$

where  $\eta_H$  stands for the corresponding Hilbert transform of the free surface elevation. Then the relationship between the local wave steepness against the current velocity, in comparison with the linear analytical solution and the results in Wu [50] is presented in Figure 4.

The figure shows that when the wave steepness is small, both the numerical results obtained by using the ESBI and HOS agree with the linear predictions. However, the results deviate from the linear theory when wave steepness becomes large, which is understandable as the contribution from the nonlinearities becomes significant. Both HOS and ESBI overpredict the steepness in following current while underestimate that in opposing current. However, the maximum differences between the obtained results by using the ESBI and HOS are about 4.6% and 4.1% for the following and opposing current, respectively, and the ESBI model slightly overpredicts the wave steepness when the flow is relatively faster. As indicated in section 2.1, the HOS suggested by Wu [50] is only accurate for modelling current interacting with small steepness waves. Therefore, the difference between the results of the two approaches is due to that the HOS had neglected higher order nonlinear terms representing the wave-current interactions. The neglected terms will become pronounced when the wave steepness increases, in which cases the HOS becomes less accurate. Nevertheless, the good agreement between the ESBI and theoretical results is observed.



(a) following current,  $U_m = 0.5c_0$

(b) opposing current,  $U_m = -0.2c_0$

Figure 4. Local wave steepness against current velocity: regular waves on collinear current

### 3.2.2 Wave blocking on opposing current

Waves propagating against an opposing current may be blocked at a certain point if the current is sufficiently strong. To validate the ESBI for simulating such situations, three cases subject to horizontally shearing current studied by Ma, et al. [61] in laboratory are selected. The cases have a variety of nonlinear scenarios. The configuration of the numerical wave tank is the same as that in section 3.1, however, the pneumatic wave maker is moved to one fourth of the tank length from the left boundary, and only the part on the right is effectively used for simulating the wave propagation in the cases.

The profile of the current is obtained by interpolating the measured velocity in laboratory, as shown by the 'Fitted' data in Figure 5, which is then prescribed to be  $\mathbf{U}$  in the ESBI simulation. The wave conditions of the selected cases are given in Table 1, where the maximum wave steepness is 0.073 (Case 1). Each simulation lasts for 400 periods, and the last 100 periods are extracted for spectral analysis by using the Fourier transform. By doing so, the local frequency ( $\omega_l$ ) corresponding to the peak of the obtained spectra at all probes along the tank can be estimated and the results are shown in Figure 6.

Table 1. Description of the configuration

Case No.	Period(s)	Wave height(cm)	Wave number ( $m^{-1}$ )
1	1.0	2.21	6.6
4	1.1	2.5	5.2
7	1.2	2.61	4.24

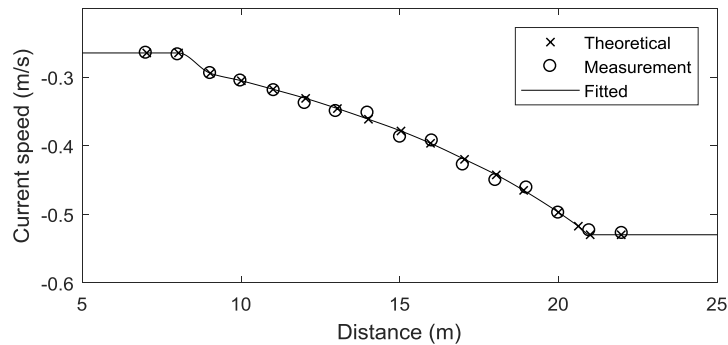


Figure 5. Profile of horizontally shearing current against distance: wave blocking on opposing current. 'Theoretical': calculated values based on continuity equation; 'Measurement': values recorded in laboratory; 'Fitted': values obtained by numerical interpolation.

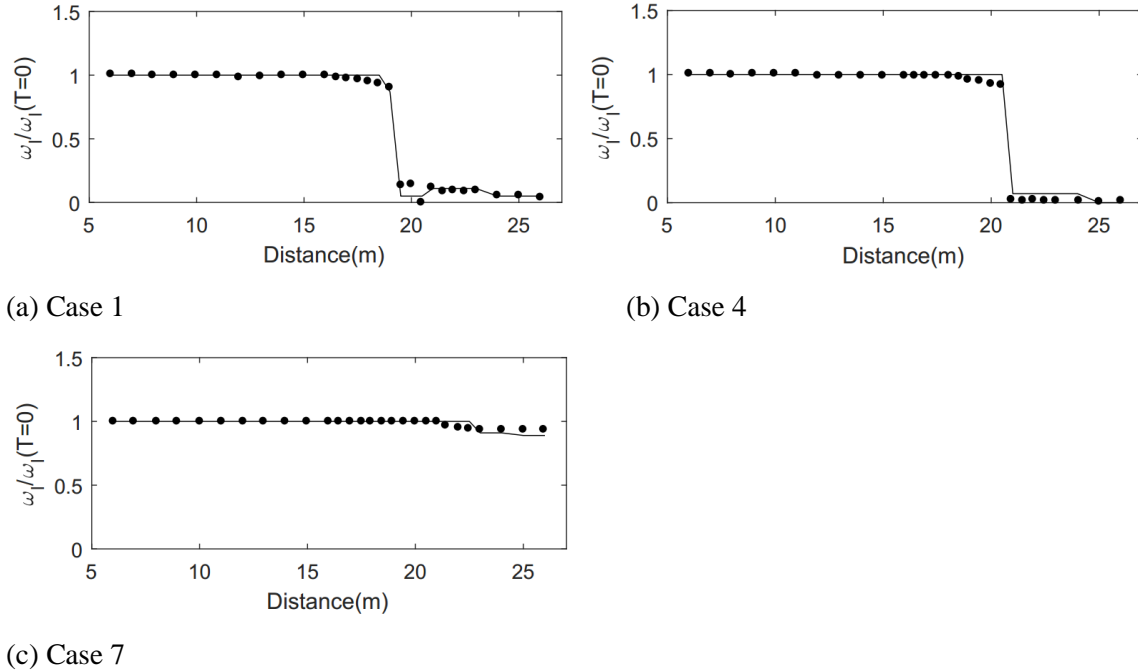


Figure 6. Local wave frequency against distance. ‘-’: ESBI; ‘•’ Measurements by Ma, et al. [61]

It can be found that in the first two cases, i.e., Case 1&4, the waves are relatively short and the phase celerity is not fast enough to compete with the current speed. Therefore, the waves are blocked at certain points. Instant frequency down-shifting is observed. For the last case, i.e., Case 7, the waves are moving sufficiently fast to penetrate the current field, despite of slight frequency down-shifting near the end of the tank. Moreover, the numerical results obtained by using the ESBI are well consistent with these measured in the laboratory. In particular, the ESBI model successfully captured the frequency down-shifting due to the blocking effects of the opposing current observed in laboratory.

In addition, the comparison of the free surface time history between the laboratory experimental data and numerical simulation results recorded at the gauges along the tank for case 1 is shown in Figure 7. It is understandable that the envelope represents the evolution of the wave energy along the tank, so that can be used to indicate the blocking effects of the current on the propagation of the waves. The figure shows that the free surface time histories predicted by the ESBI agree reasonably with the experimental data, though the measured free surface in laboratory behaves irregularly, which may be caused by the imperfection for reproducing steady current condition, e.g., the turbulence of the current as observed [61]. However, the blockage of the waves due to the opposing current is successfully captured by the ESBI model.

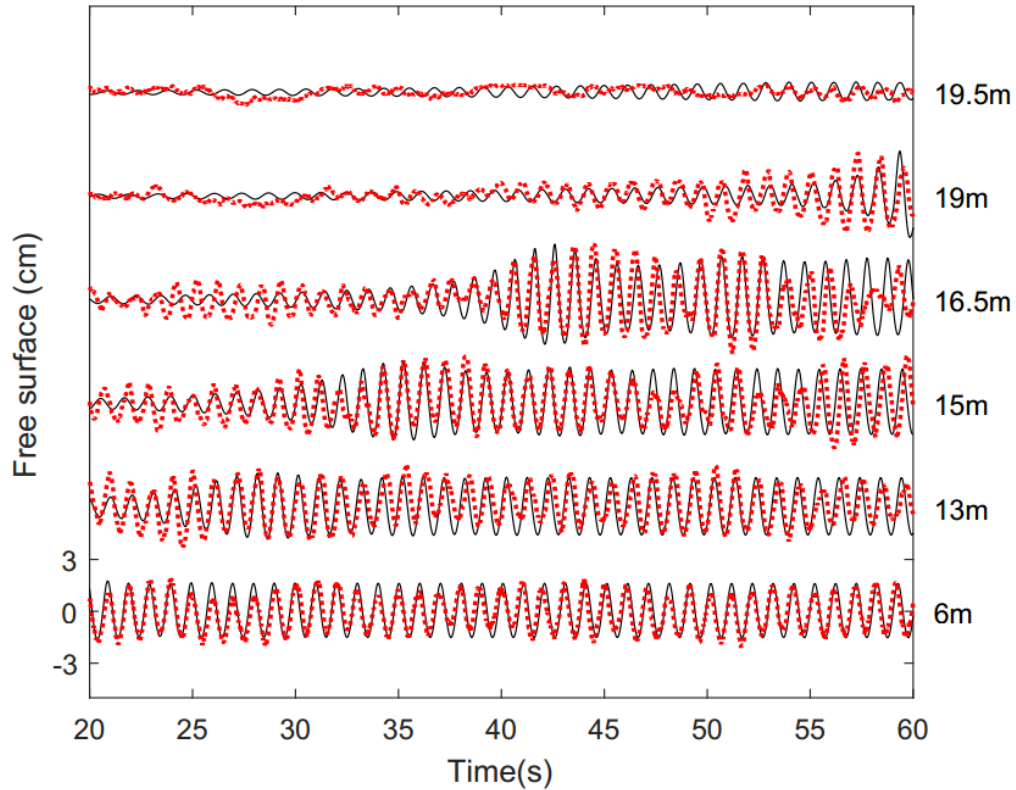


Figure 7. Comparison of the time histories of the surface elevation for case 1 of wave steepness 0.073. ‘—’: free surface by ESBI, ‘· · ·’: laboratory measurement in [61].

### 3.3 Three-dimensional Horizontally-shearing current

In addition to the two-dimensional validation cases, three-dimensional simulations are also performed to demonstrate the robustness and effectiveness of the newly developed ESBI method, for modelling waves interacting with horizontally-shearing current. Waves propagating on an oblique current is more complicated. It was firstly studied by Shyu and Tung [10] by using the ray theory. Subsequently, Lavrenov [3] analyzed the ray pattern of the Agulhas current and found that the rogue waves can be generated at the focusing point where wave energy concentrates. Later studies pointed out that wave-current interaction is the major mechanism of the rogue wave phenomenon in deep water [9, 62]. Hereafter, two cases are considered, i.e., the modulation instability induced by oblique opposing current, and the spreading seas entering a horizontally-shearing current field. The simulations of the selected two cases have been performed in a physical wave tank by Toffoli, et al. [63]. These cases will be reproduced by using the ESBI method and the obtained results will be compared with the laboratory data.

### 3.3.1 Modulation instability

The NWT covers 78m×58m in space and is resolved into 2048×512 collocation points, whilst the directional wave maker is installed at one fourth of the total length from the left boundary. Waves are absorbed at far ends and only the part on the right of the wave maker is effectively used. Three components are input to generate the wave maker signal, where the steepness of the main wave (carrier wave) is 0.1 and period 0.8s, including two side-bands with 1/4 the amplitude of carrier wave and bandwidth equals to 0.25.

The current flows obliquely in an angle of  $\Psi = 110^\circ$  with respect to the main wave direction. The configuration of the NWT is shown in Figure 8. The maximum current speed is 0.2m/s near the centre of the wave tank, however, exact values of the current speed is unavailable except the measurements at five individual current meters. To initialize the current field in the ESBI, the current profile is approximated by using

$$|U| = \begin{cases} -0.104, & X/L_0 \leq 5 \\ -0.104 - 0.027 \times H((12 - X/L_0)/7), & 5 < X/L_0 \leq 12 \\ -0.131, & 12 < X/L_0 \leq 17 \\ -0.104 - 0.027 \times H((X/L_0 - 17)/7), & 17 < X/L_0 \leq 24 \\ -0.104, & X/L_0 > 24 \end{cases} \quad (39)$$

It is found the fitted results agree very well with the measurement in Toffoli, et al. [63], as shown in Figure 9, where the maximum error is about 2.0%.

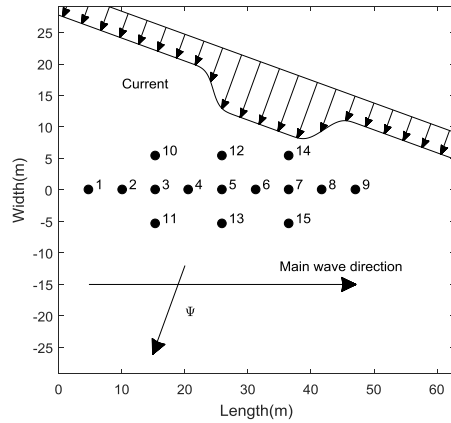


Figure 8. Configuration of the NWT

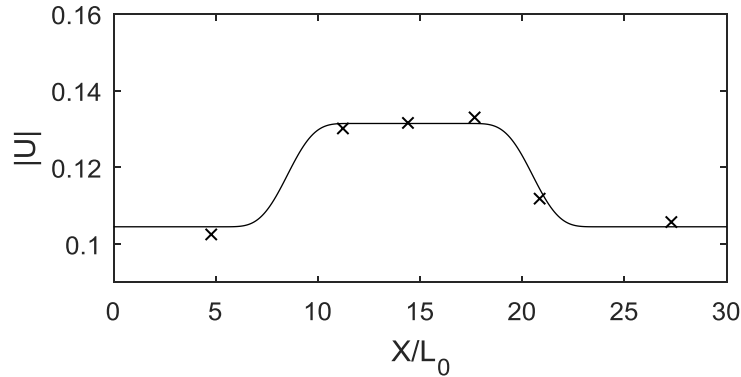
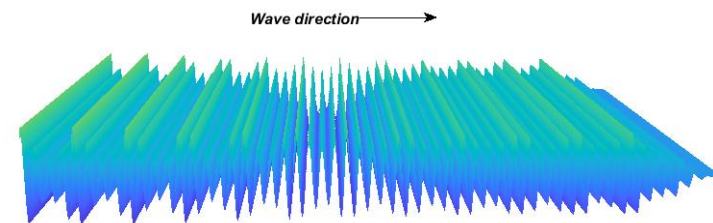
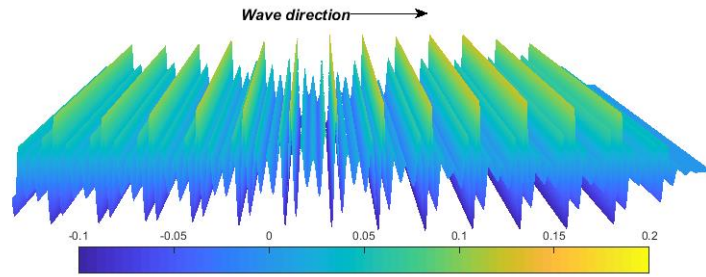


Figure 9. Fitted profile of the current speed. 'x': Measured in Toffoli, et al.[63]; '—': Fitted.

The three-dimensional free surface distributions in space at the end of the simulation are shown in Figure 10 for the cases with and without the current. It can be found in Figure 10 (a) that around 11.5 wave groups coexist in the computational domain when current is not present. However, as shown in Figure 10 (b), due to the current effects, the waves are compressed and 13 groups are observed in the NWT simultaneously. Meanwhile, the wave heights are found larger than those in absence of current. In addition, during the simulation, the data of the free surface elevation are collected at 9 wave gauges along the main wave direction, and the comparison of the time histories of the free surface elevation between the numerical results and that reported in Toffoli, et al. [63] is shown in Figure 11. It is found that without the current, since the wave train features a small Benjamin-Feir Index, the modulation instability cannot develop into extreme waves during the propagation. Whereas the waves are compressed due to the presence of opposing current, which increases the Benjamin-Feir Index, thus the instability is triggered and the maximum free surface is achieved around gauge #5 and #6. Meanwhile, the ESBI successfully captured the variation of the surface elevation at different locations and the results agree quite well with the laboratory experiment in both the cases with and without current. However, it should be noted that in the case with current, the time series measured in physical tank are more erratic than the ones in NWT, which is presumably related to the turbulence fluctuation of the current velocity [63]. Nevertheless, the evolution of the wave packet predicted by the numerical results is qualitatively consistent with the laboratory observations.



(a) without current (the initial carrier wave steepness is 0.1)



(b) with current

Figure 10. The spatial distribution of modulated free surface at  $T/T_0 = 150$  (Color online)

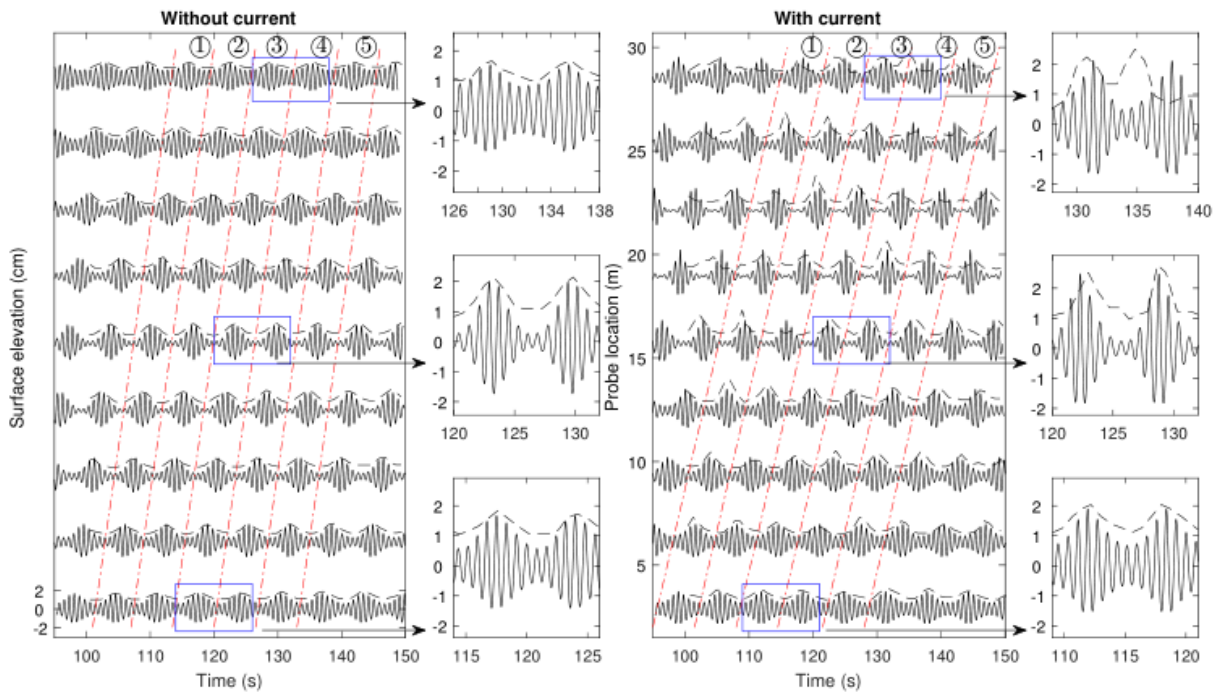


Figure 11. Comparison of the time histories of the surface elevation. ‘-’: free surface by ESBI, ‘- -’: surface envelope in Toffoli, et al. [63] (Color online).

To further demonstrate the robustness of the ESBI quantitatively, the propagation of 5 individual wave groups are tracked, as shown in Figure 11 between the dash lines. Their maximum crests recorded at each probe are extracted, which are then normalized by the concurrent variances and shown in Figure 12. To remove the erratic feature of the data collected in the laboratory, the mean value is estimated by averaging the values indicated by the 5 curves, and is also displayed in the figure. Meanwhile, the numerical data is identical among each individual wave group, thus only the mean value is displayed and compared with that in laboratory. It is found that the maximum crest height observed in the NWT quantitatively agrees quite

well with that in Toffoli, et al. [63], where the maximum error between the numerical results and the mean value of laboratory observation in presence of current is about 9.8% at gauge #5. The good agreement reveals that the present ESBI model successfully captured the dynamics of the unstable wave train.

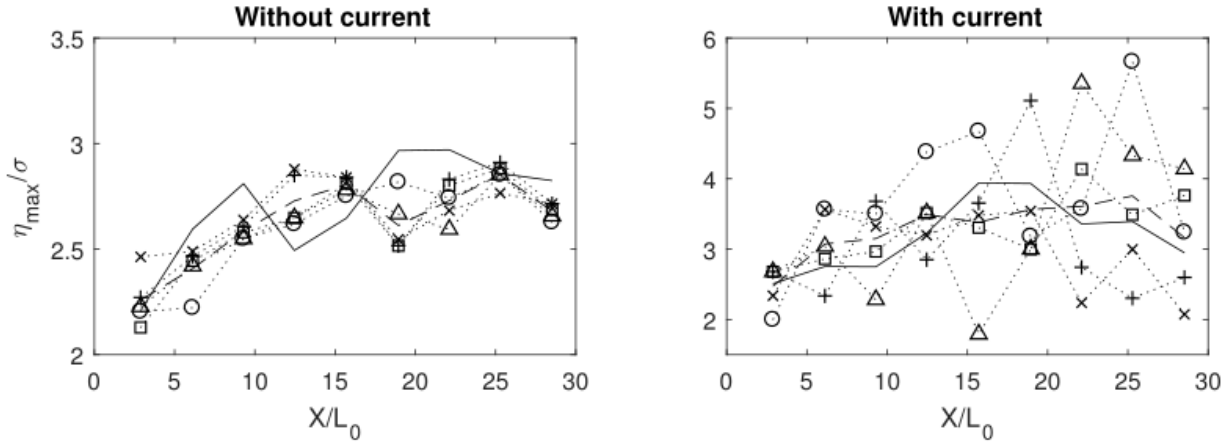


Figure 12. Comparison of the maximum free surface against location. ‘·····’: Group (1) in [63]; ‘···Δ···’: Group (2) in [63]; ‘···□···’: Group (3) in [63]; ‘···+···’: Group (4) in [63]; ‘···×···’: Group (5) in [63]; ‘---’: Average in [63]; ‘—’: ESBI.

### 3.3.2 Spreading seas

To show that the present model is not limited to only model regular waves in three dimensions, it is then verified for simulating spreading seas with presence of horizontally shearing current. The configuration of the NWT is the same with that in section 3.3.1, and the JONSWAP spectrum is employed, where the peak period is 1s, significant wave height 0.08m and peak enhancement factor 6. The spreading function is chosen as

$$G(\theta) = \frac{\Gamma(N/2 + 1)}{\sqrt{\pi}\Gamma[(N + 1)/2]} \cos^N(\theta) \quad (40)$$

where  $\Gamma()$  is the Gamma function and  $N = 24$ . The mean wave direction, the current velocity and direction are both the same with that in section 3.3.1.

Snapshots of the free surface elevation in space at  $T/T_0 = 150$  are presented in Figure 13, in which a qualitative comparison between Figure 13(a) and (b) reveals that the number of extreme waves in presence of current are more than that without current presence. This is understandable as the opposing current can contribute to the probability of extreme wave events [1]. To examine the accuracy of the numerical model quantitatively, simulated results are compared with that in Toffoli, et al. [63]. Since time history of the free

surface is unavailable and direct comparison of the surface elevation cannot be made, only the kurtosis at different locations along the main wave direction is analyzed. It is estimated by using the formula

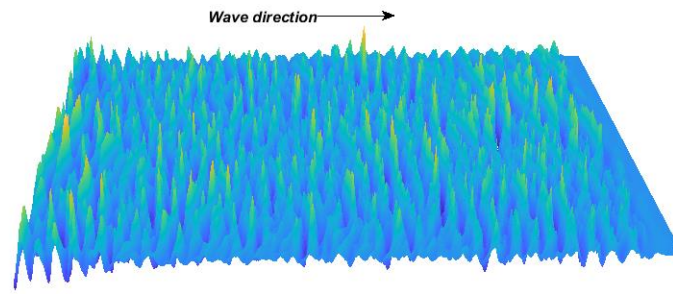
$$\kappa_4 = m_4/m_2^2 \quad (41)$$

where  $m_4$  and  $m_2$  are the fourth and second moment of the surface time history, respectively. In fact, the kurtosis reflects the probability of the extreme waves in random wave field [1], thus is sufficient to examine the enhancement of the nonlinearities of the wave field due to the current. Based on the linear theory, when the wave steepness is small, the statistics of the random sea follows the Gaussian distribution, which makes kurtosis identical to 3. However, when the wave steepness increases, the nonlinearities become stronger and the kurtosis will exceed 3. To approximate the kurtosis while considering nonlinear effects up to the second order, a formula is suggested by Longuet-Higgins [64] as below

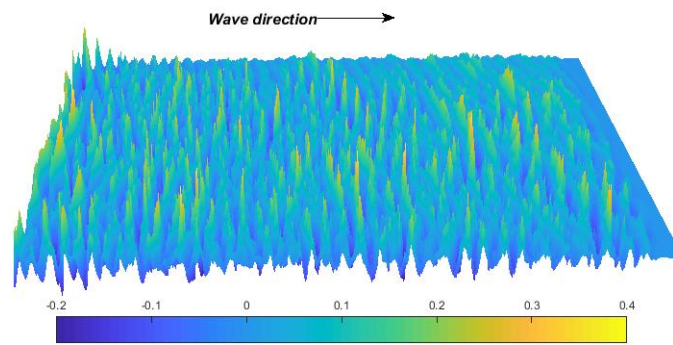
$$\kappa'_4 = 3 + 24\sigma^2 \quad (42)$$

and  $\sigma$  is the standard deviation of the surface elevation.

The results obtained by using the numerical simulation, together with that estimated by using Eq. (42) and obtained in the physical wave tank [63] are presented in Figure 14. It shows good agreement between the curves obtained numerically and experimentally. Moreover, it is observed that the kurtosis is subjected to a deceleration of its growth throughout the propagation, meanwhile, shows the tendency to preserve slightly higher values with current presence. At the far end from the wave maker, the kurtosis agrees very well with the second order prediction without the current, whereas it is significantly underestimated when current is involved. In the middle part of the tank, the results of Eq. (42) is close to the experimental data of the cases with current. However, the difference between the values of the kurtosis with and without the current is successfully captured by the numerical simulation. These results demonstrated that Eq. (42) may not correctly reflect the evolution of the kurtosis throughout the whole tank. In addition, the errors of the maximum kurtosis between the results obtained in the NWT and physical wave tanks are 0.8% and 1.7% corresponding to the cases without and with current, respectively. These indicate that the present ESBI model is very accurate when employed to model the property of irregular waves in presence of current.



(a) without current



(b) with current

Figure 13. The spatial distribution of spreading wave free surface at  $T/T_0 = 150$  (Color online)

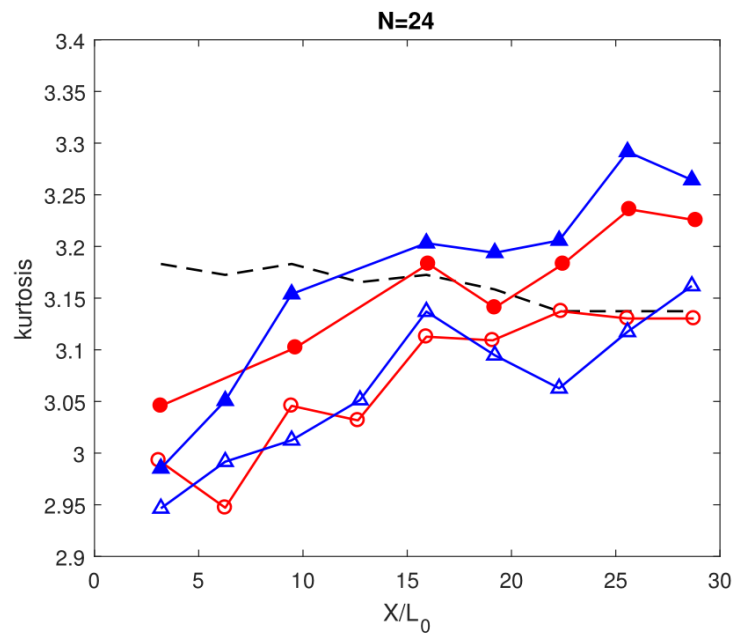


Figure 14. Kurtosis against probe location (Color online). ' - - ': with current, 2nd order;

'—○—': without current, Toffoli, et al.[63]; '—●—': with current, Toffoli, et al. [63]; '—△—': without current, ESBI; '—▲—': with current, ESBI.

## 4 Conclusion

This study suggests an accurate and efficient phase-resolved numerical method to model the fully nonlinear three-dimensional interactions between waves and horizontally varying current. To achieve this goal, a new system of equations describing the fully nonlinear interactions between waves and varying current is proposed, removing the limitation to the small wave steepness of the existing formulation in literature. The Enhanced Spectral Boundary Integral (ESBI) Method is extended to solve the problems based on the new equations by considering the extra terms associated with wave-current interaction. The newly developed method can be employed to simulate the real evolution of ocean waves on current, which may not be done correctly by the existing methods in literature.

The newly developed method based on the new equations is compared with experimental data available in literature in the several cases, including two-dimensional focusing waves on an uniform current, two-dimensional regular waves interacting with spatially-varying current and three-dimensional interaction of horizontal varying current with spreading ocean waves and modulated waves generated by superposing two-sideband wave components onto a carrier wave component. It is found in two dimensions that the release of the focusing wave packet on the following uniform current was lagged, while it was reversed on the opposing uniform current. When waves were subjected to horizontally shearing current, instant frequency down-shifting of the wave train along the tank was observed, due to the blockage of the opposing current. In addition, when waves propagated opposed to oblique horizontally shearing current in three dimensions, modulated uniform wave train featuring small Benjamin-Feir index could develop into large steepness waves due to modulation instability. Apart from these, the kurtosis of the spreading random sea was shown to preserve slightly higher values with current presence. It is also found that generally good agreement between the numerical results from the newly developed method and laboratory measurements is achieved in all the cases considered. This indicates that the method works well when it is employed to model the two or three dimensional, fully nonlinear wave-current interactions in the cases with uniform or horizontally sheared current. Furthermore, the phase of each individual wave is resolved, so that not only the statistical information, but also the kinematics and dynamics of the fully nonlinear wave-current field can be obtained, which are of great importance for the sake of engineering purposes.

As demonstrated in section 3.2.1, the some differences between the results obtained with the HOS and the ESBI model are observed when waves becomes steep. The reasons causing the differences might be

attributed to the nature of the HOS approach, i.e., the formulations suggested by Dommermuth and Yue [65] as those employed by Wu [50]. On one hand, the HOS model did not account for higher order nonlinear terms representing wave-current interactions. On the other hand, it fails to preserve the Hamiltonian structure of the prognostic equations[66], of which the insufficiency is reported for modeling long-time wave propagation [67]. Although it can be improved by employing another version of the HOS suggested by West, et al. [68], further investigations are required.

Nevertheless, the limitation of the present model is that it can only be used to model non-breaking waves, as the methodology itself is based on the potential theory that assumes the water is inviscid and irrotational. In the future study, the present model will be coupled with other methods which can deal with the breaking waves to overcome the drawback. Moreover, the present model may be insufficient for modeling waves subject to strong vertically shearing current, which is important for studying waves near shore and in coastal areas. In the future, the present ESBI model will be extended to include this feature, based perhaps on the work by Fructus and Grue [69], in which variable bathymetry is considered.

## Acknowledgements

The authors gratefully acknowledge the financial support of EPSRC, UK (EP/N006569/1, EP/N008863/1 and EP/M022382/1) and DST-UKIERI project (DST-UKIERI-2016-17-0029). The authors also appreciate Dr. Yuxiang Ma for providing the experimental data.

## Appendix

The formulas for estimating  $V_3$  and  $V_4$  are presented here without further details but can be found in [55], where the convolution part of  $V_3$  is given by

$$\begin{aligned}
 F \{V_3^{(1)}\} = & -\frac{K}{6} \left[ Ki\mathbf{K} \cdot F\{\zeta^3 \nabla \tilde{\phi}\} - 3F \left\{ \zeta F^{-1} \left\{ Ki\mathbf{K} \cdot F\{\zeta^2 \nabla \tilde{\phi}\} \right\} \right\} \right. \\
 & \left. + 3F \left\{ \zeta^2 F^{-1} \left\{ Ki\mathbf{K} \cdot F\{\zeta \nabla \tilde{\phi}\} \right\} \right\} + F \left\{ \zeta^3 F^{-1} \left\{ K^3 F\{\tilde{\phi}\} \right\} \right\} \right]
 \end{aligned} \tag{A. 1}$$

$$\begin{aligned}
F\{V_3^{(2)}\} = & -\frac{K}{120} \left[ i\mathbf{K}K^3 \cdot F\{\zeta^5 \nabla \tilde{\phi}\} - 5F\{\zeta F^{-1}\{i\mathbf{K}K^3 \cdot F\{\zeta^4 \nabla \tilde{\phi}\}\}\} \right. \\
& + 10F\{\zeta^2 F^{-1}\{i\mathbf{K}K^3 \cdot F\{\zeta^3 \nabla \tilde{\phi}\}\}\} \\
& - 10F\{\zeta^3 F^{-1}\{i\mathbf{K}K^3 \cdot F\{\zeta^2 \nabla \tilde{\phi}\}\}\} \\
& \left. + 5F\{\zeta^4 F^{-1}\{i\mathbf{K}K^3 \cdot F\{\zeta \nabla \tilde{\phi}\}\}\} + F\{\zeta^5 F^{-1}\{K^5 F\{\tilde{\phi}\}\}\} \right]
\end{aligned} \tag{A. 2}$$

and the integration part

$$\begin{aligned}
F\{V_{3,I}\} = & \frac{K}{2\pi} F \left\{ \frac{35}{16} \int \tilde{\phi}' \nabla' \cdot \left[ (\zeta' - \zeta) \nabla' \frac{1}{R} \right] D^6 d\mathbf{X}' \right. \\
& + \int \tilde{\phi}' \left[ 1 - (1 + D^2)^{-3/2} - \frac{3}{2} D^2 + \frac{15}{8} D^4 - \frac{35}{16} D^6 \right] \nabla' \\
& \left. \cdot \left[ (\zeta' - \zeta) \nabla' \frac{1}{R} \right] d\mathbf{X}' \right\}
\end{aligned} \tag{A. 3}$$

Meanwhile, the convolution part  $V_4$  is given by

$$F\{V_4^{(1)}\} = -\frac{K}{2} \left[ KF\{\zeta^2 V\} - 2F\{\zeta F^{-1}\{KF\{\zeta V\}\}\} + F\{\zeta^2 F^{-1}\{KF\{V\}\}\} \right] \tag{A. 4}$$

$$\begin{aligned}
F\{V_4^{(2)}\} = & -\frac{K}{24} \left[ K^3 F\{V\zeta^4\} - 4F\{\zeta F^{-1}\{K^3 F\{V\zeta^3\}\}\} + 6F\{\zeta^2 F^{-1}\{K^3 F\{V\zeta^2\}\}\} \right. \\
& \left. - 4F\{\zeta^3 F^{-1}\{K^3 F\{V\zeta\}\}\} + F\{\zeta^4 F^{-1}\{K^3 F\{V\}\}\} \right]
\end{aligned} \tag{A. 5}$$

$$\begin{aligned}
F\{V_4^{(3)}\} = & \frac{-K}{720} \left[ K^5 F\{V\zeta^6\} - 6F\{\zeta F^{-1}\{K^5 F\{V\zeta^5\}\}\} \right. \\
& + 15F\{\zeta^2 F^{-1}\{K^5 F\{V\zeta^4\}\}\} - 20F\{\zeta^3 F^{-1}\{K^5 F\{V\zeta^3\}\}\} \\
& + 15F\{\zeta^4 F^{-1}\{K^5 F\{V\zeta^2\}\}\} - 6F\{\zeta^5 F^{-1}\{K^5 F\{V\zeta\}\}\} \\
& \left. + F\{\zeta^6 F^{-1}\{K^5 F\{V\}\}\} \right]
\end{aligned} \tag{A. 6}$$

and the integration part

$$F\{V_{4,I}\} = \frac{K}{2\pi} F \left\{ \int \frac{V'}{R} \left( 1 - \frac{1}{\sqrt{1+D^2}} - \frac{1}{2} D^2 + \frac{3}{8} D^4 - \frac{5}{16} D^6 \right) d\mathbf{X}' \right\} \tag{A. 7}$$

## References

- [1] C. Kharif, E. Pelinovsky and A. Slunyaev, *Rogue Waves in the Ocean*, Berlin Heidelberg:

Springer-Verlag, 2009.

- [2] M. Gerber, The interaction of deep-water gravity waves and an annular current: linear theory, *Journal of Fluid Mechanics*. 248 (1993) 153-172.
- [3] I. V. Lavrenov, The wave energy concentration at the Agulhas current off South Africa, *Natural Hazards*. 17 (2) (1998) 117-127.
- [4] I. V. Lavrenov and A. V. Porubov, Three reasons for freak wave generation in the non-uniform current, *European Journal of Mechanics-B/Fluids*. 25 (5) (2006) 574-585.
- [5] D. H. Peregrine, Interaction of water waves and currents, *Advances in Applied Mechanics*. 16 (1976) 9-117.
- [6] G. P. Thomas, Wave-current interactions: an experimental and numerical study. Part 1. Linear waves, *Journal of Fluid Mechanics*. 110 (1981) 457-474.
- [7] G. P. Thomas, Wave-current interactions: an experimental and numerical study. Part 2. Nonlinear waves, *Journal of Fluid Mechanics*. 216 (1990) 505-536.
- [8] J. H. Shyu and O. M. Phillips, The blockage of gravity and capillary waves by longer waves and currents, *Journal of Fluid Mechanics*. 217 (1990) 115-141.
- [9] B. S. White and B. Fornberg, On the chance of freak waves at sea, *Journal of Fluid Mechanics*. 355 (1998) 113-138.
- [10] J. H. Shyu and C. C. Tung, Reflection of oblique waves by currents: analytical solutions and their application to numerical computations, *Journal of Fluid Mechanics*. 396 (1999) 143-182.
- [11] I. G. Jonsson, C. Skougaard and J. D. Wang, Interaction between waves and currents, *Coastal Engineering*. (1970) 489-507.
- [12] I. G. Jonsson, Wave-current interactions, *Ocean Engineering Science: The Sea*. 9 (A) (1990) 65-120.
- [13] S. B. Yoon and P. L. F. Liu, Interactions of currents and weakly nonlinear water waves in shallow water, *Journal of fluid mechanics*. 205 (1989) 397-419.
- [14] Q. Chen, P. A. Madsen, H. A. Schäffer and D. R. Basco, Wave-current interaction based on an enhanced Boussinesq approach, *Coastal Engineering*. 33 (1) (1998) 11-39.
- [15] W. Chen, V. Panchang and Z. Demirbilek, On the modeling of wave–current interaction using

- the elliptic mild-slope wave equation, *Ocean Engineering*. 32 (17) (2005) 2135-2164.
- [16] M. F. Gobbi, J. T. Kirby and G. E. Wei, A fully nonlinear Boussinesq model for surface waves. Part 2. Extension to  $O(kh)^4$ , *Journal of Fluid Mechanics*. 405 (2000) 181-210.
- [17] P. J. Lynett, A multi-layer approach to modeling generation, propagation, and interaction of water waves (PhD thesis), New York: Cornell University, 2002.
- [18] M. Isaacson and K. F. Cheung, Time-domain solution for wave—current interactions with a two-dimensional body, *Applied Ocean Research*. 15 (1) (1993) 39-52.
- [19] D. J. Kim and M. H. Kim, Wave-Current-Body Interaction by a Time-Domain High-Order Boundary Element Method. Honolulu, 1997.
- [20] P. Ferrant, Runup on a cylinder due to waves and current: potential flow solution with fully nonlinear boundary conditions, *International Journal of Offshore and Polar Engineering*. 11 (1) (2001) 1-9.
- [21] S. Ryu, M. H. Kim and P. J. Lynett, Fully nonlinear wave-current interactions and kinematics by a BEM-based numerical wave tank, *Computational Mechanics*. 32 (4-6) (2003) 336-346.
- [22] R. M. Moreira and D. H. Peregrine, Nonlinear interactions between deep-water waves and currents, *Journal of Fluid Mechanics*. 691 (2012) 1-25.
- [23] S. Yan, Q. W. Ma and T. A. A. Adcock, Investigations of freak waves on uniform current, Harbin, 2010.
- [24] D. G. Dommermuth and D. K. Yue, The nonlinear three-dimensional waves generated by a moving surface disturbance. Hague, Netherlands, 1988.
- [25] J. Grue and A. Jensen, Orbital velocity and breaking in steep random gravity waves, *Journal of Geophysical Research: Oceans*. 117 (C7) (2012) 0148-0227.
- [26] J. C. Park, M. H. Kim and H. Miyata, Three-dimensional numerical wave tank simulations on fully nonlinear wave—current—body interactions, *Journal of Marine Science and Technology*. 6 (2) (2001) 70-82.
- [27] H. C. Chen and K. Yu, CFD simulations of wave—current—body interactions including greenwater and wet deck slamming, *Computers & Fluids*. 38 (5) (2009) 970-980.
- [28] J. S. Zhang, Y. Zhang, D. S. Jeng, P. F. Liu and C. Zhang, Numerical simulation of wave—current interaction using a RANS solver, *Ocean Engineering*. 75 (2014) 157-164.

- [29] F. P. Bretherton and C. J. Garrett, Wavetrains in inhomogeneous moving media, *Proceedings of the Royal Society of London A: Mathematical, Physical and Engineering Sciences*. 302 (1471) (1968) 529-554.
- [30] R. A. Dalrymple, A finite amplitude wave on a linear shear current, *Journal of Geophysical Research*. 79 (30) (1974) 4498-4504.
- [31] J. A. Simmen and P. G. Saffman, Steady Deep Water Waves on a Linear Shear Current, *Studies in Applied Mathematics*. 73 (1) (1985) 35-57.
- [32] A. T. Da Silva and D. H. Peregrine, Steep, steady surface waves on water of finite depth with constant vorticity, *Journal of Fluid Mechanics*. 195 (1988) 281-302.
- [33] N. Kishida and R. J. Sobey, Stokes theory for waves on linear shear current, *Journal of Engineering Mechanics*. 114 (8) (1988) 1317-1334.
- [34] A. Constantin and W. Strauss, Exact steady periodic water waves with vorticity, *Communications on Pure and Applied Mathematics*. 57 (4) (2004) 481-527.
- [35] O. S. Pak and K. W. Chow, Free surface waves on shear currents with non-uniform vorticity: third-order solutions, *Fluid Dynamics Research*. 41 (3) (2009) 035511.
- [36] W. Choi, Nonlinear surface waves interacting with a linear shear current, *Mathematics and Computers in Simulation*. 80 (1) (2009) 29-36.
- [37] O. G. Nwogu, Interaction of finite-amplitude waves with vertically sheared current fields, *Journal of Fluid Mechanics*. 627 (2009) 179-213.
- [38] A. Constantin and E. Varvaruca, Steady periodic water waves with constant vorticity: regularity and local bifurcation, *Archive for Rational Mechanics and Analysis*. 199 (1) (2011) 33-67.
- [39] V. Kozlov and N. Kuznetsov, Dispersion equation for water waves with vorticity and Stokes waves on flows with counter-currents, *Archive for Rational Mechanics and Analysis*. 214 (3) (2014) 971-1018.
- [40] R. Ribeiro, P. A. Milewski and A. Nachbin, Flow structure beneath rotational water waves with stagnation points, *Journal of Fluid Mechanics*. 812 (2017) 792-814.
- [41] M. Francius and C. Kharif, Two-dimensional stability of finite-amplitude gravity waves on water of finite depth with constant vorticity, *Journal of Fluid Mechanics*. 830 (2017) 631-

- [42] H. Tamura, T. Waseda, Y. Miyazawa and K. Komatsu, Current-induced modulation of the ocean wave spectrum and the role of nonlinear energy transfer, *Journal of Physical Oceanography*. 38 (12) (2008) 2662-2684.
- [43] F. M. Turpin, C. Benmoussa and C. C. Mei, Effects of slowly varying depth and current on the evolution of a Stokes wavepacket, *Journal of Fluid Mechanics*. 132 (1983) 1-23.
- [44] M. Gerber, The Benjamin-Feir instability of a deep-water Stokes wavepacket in the presence of a non-uniform medium, *Journal of Fluid Mechanics*. 176 (1987) 311-332.
- [45] A. V. D. Cornelis, The effect of non-uniformity of modulated wavepackets on the mechanism of benjamin-feir instability, *Journal of Fluid Mechanics*. 399 (1999) 237-249.
- [46] T. T. Janssen and T. H. C. Herbers, Nonlinear wave statistics in a focal zone, *Journal of Physical Oceanography*. 39 (8) (2009) 1948-1964.
- [47] K. B. Hjelmervik and K. Trulsen, Freak wave statistics on collinear currents, *Journal of Fluid Mechanics*. 637 (2009) 267-284.
- [48] J. R. Stocker and D. H. Peregrine, The current-modified nonlinear Schrödinger equation, *Journal of Fluid Mechanics*. 399 (1999) 335-353.
- [49] J. Wang, Q. Ma and S. Yan, On quantitative errors of two simplified unsteady models for simulating unidirectional nonlinear random waves on large scale in deep sea, *Physics of Fluids*. 29 (6) (2017) 067107.
- [50] G. Wu, Direct Simulation and Deterministic Prediction of Large-scale Nonlinear Ocean Wave-field (PhD Thesis), Massachusetts, USA: Massachusetts Institute of Technology, 2004.
- [51] D. Clamond and J. Grue, A fast method for fully nonlinear water-wave computations, *Journal of Fluid Mechanics*. 447 (2001) 337-355.
- [52] D. Fructus, D. Clamond, J. Grue and O. Kristiansen, An efficient model for three-dimensional surface wave simulations Part I: Free space problems, *Journal of Computational Physics*. 205 (2005) 665-685.
- [53] D. Clamond, D. Fructus, J. Grue and O. Kristiansen, An efficient model for three-dimensional surface wave simulations. Part II: Generation and absorption, *Journal of*

Computational Physics. 205 (2005) 686-705.

- [54] J. Grue, Computation formulas by FFT of the nonlinear orbital velocity in three-dimensional surface wave fields, *J. Eng. Math.* 67 (2010) 55-69.
- [55] J. Wang and Q. W. Ma, Numerical techniques on improving computational efficiency of Spectral Boundary Integral Method, *International Journal for Numerical Methods in Engineering.* 102 (10) (2015) 1638-1669.
- [56] D. Fructus, C. Kharif, M. Francius, Ø. Kristiansen, D. Clamond and J. Grue, Dynamics of crescent water wave patterns, *Journal of Fluid Mechanics.* 537 (2005) 155-186.
- [57] P. P. Sullivan and J. C. McWilliams, Dynamics of winds and currents coupled to surface waves, *Annual Review of Fluid Mechanics.* 42 (2010) 19-42.
- [58] J. Grue and J. Kolaas, Experimental particle paths and drift velocity in steep waves at finite water depth, *Journal of Fluid Mechanics.* 810 (2017) R1.
- [59] J. Wang and Q. W. Ma, Numerical Investigation on Limitation of Boussinesq Equation for Generating Focusing Waves, *Procedia Engineering.* 126 (2015) 597-601.
- [60] C. H. Wu and A. Yao, Laboratory measurements of limiting freak waves on currents, *Journal of Geophysical Research: Oceans.* 109 (2004) C12002.
- [61] Y. Ma, G. Dong, M. Perlin, X. Ma, G. Wang and J. Xu, Laboratory observations of wave evolution, modulation and blocking due to spatially varying opposing currents, *Journal of Fluid Mechanics.* 661 (2010) 108-129.
- [62] A. Toffoli, J. M. Lefevre, E. Bitner-Gregersen and J. Monbaliu, Towards the identification of warning criteria: analysis of a ship accident database, *Applied Ocean Research.* 27(6) (2005) 281-291.
- [63] A. Toffoli, L. Cavaleri, A. Babanin, M. Benoit, E. Bitner-Gregersen, J. Monbaliu, M. Onorato, A. Osborne and C. Stansberg, Occurrence of extreme waves in three-dimensional mechanically generated wave fields propagating over an oblique current, *Natural Hazards and Earth System Sciences.* 11 (3) (2011) 895-903.
- [64] M. S. Longuet-Higgins, The effect of non-linearities on statistical distributions in the theory of sea waves, *Journal of Fluid Mechanics.* 17 (3) (1963) 459-480.
- [65] D. G. Dommermuth and D. K. Yue, A high-order spectral method for the study of nonlinear

gravity waves, *Journal of Fluid Mechanics*. 184 (1987) 267-288.

- [66] J. Touboul and C. Kharif, Numerical simulations of water waves' modulational instability under the action of wind and dissipation, in: *Numerical Simulation-From Theory to Industry*, InTech, 2012.
- [67] D. Clamond, M. Francius, J. Grue and C. Kharif, Long time interaction of envelope solitons and freak wave formations, *European Journal of Mechanics-B/Fluids*. 25 (5) (2006) 536-553.
- [68] B. J. West, K. A. Brueckner, R. S. Janda, D. M. Milder, R. L. Milton, A new numerical method for surface hydrodynamics, *Journal of Geophysical Research: Oceans*. 92 (C11) (1987) 11803-11824.
- [69] D. Fructus and J. Grue, An explicit method for the nonlinear interaction between water waves and variable and moving bottom topography, *Journal of Computational Physics*. 222 (2) (2007) 720-739.